Journal of Alloys and Compounds 509 (2011) 7027–7033

Contents lists available at ScienceDirect

Journal of Alloys and Compounds

journal homepage: www.elsevier.com/locate/jallcom

High-temperature oxidation behavior of Nb–Si–Cr alloys with Hf additions

Alma Vazquez, S.K. Varma*

Department of Metallurgical and Materials Engineering, The University of Texas at El Paso, El Paso, TX 79968-0520, USA

ARTICLE INFO

Article history:
Received 7 January 2011
Received in revised form 25 February 2011
Accepted 28 February 2011
Available online 8 March 2011

Keywords:
Oxidation
XRD
Niobium alloys
High-temperature alloys
Hafnium

ABSTRACT

The oxidation behavior of two alloys from the Nb–Si–Cr system containing hafnium has been investigated under isothermal and cyclic conditions. Nb–20Si–20Cr–(5,10)Hf alloys (composition in atomic percent) were exposed to air for 24 and 168 h over a range of temperatures from 700 °C to 1400 °C. A gravimetric method was used to determine the oxidation kinetics; weight gain per unit area as a function of temperature or time. Computed isothermal sections of the quaternary Nb–Si–Cr–Hf phase diagrams were used for alloy selection. XRD, SEM and EDS were used to characterize the phases present in the oxidation products and the alloys. Oxidation experiments revealed extremely good oxidation resistance at 700 °C and 800 °C and above 1200 °C under isothermal conditions for both alloys. Partial pesting was observed when the samples were exposed to 800 °C. Complete oxide formation was observed above 1000 °C for 5Hf and above 900 °C for 10Hf up to 1200 °C. Beneficial effects have been observed with the addition of 10Hf to the alloy compared to 5Hf at 700 °C, 1200 °C and 1300 °C resulting in a reduction of weight gain per unit area.

1. Introduction

The high-temperature material performance requirements have been increasing recently due to improvements in aircraft engine and gas turbine system designs. Nickel-based superalloys are reaching their maximum operating surface temperatures of 1150 °C; therefore high-temperature materials that can operate at the new elevated service temperature limits are desired. Promising materials for structural applications include Nb-based multiphase alloys due to the balance of properties such as low density, high melting points and high-temperature strength [1].

Attempts have been made to prepare the alloys of Nb–Si with chromium, hafnium, aluminum, and tin additions to create complex multiphase alloys in order to achieve the new high-temperature standards [2–13]. Geng et al. [9] have studied the oxidation of Nb–Si–Cr–Al system that showed inferior oxidation resistance than Ni-based superalloys. The research consisted of using different alloying elements and studying the effects on the oxidation behavior. Even though the addition of Hf did not change the oxidation kinetics at 800 °C it reduced the oxidation rate at 1200 °C. Moreover, the additions of reactive elements (e.g. yttrium, zirconium, hafnium, and cerium) have improved the high-temperature oxidation behavior of alumina-forming alloys [14]. The incorporation of yttrium and hafnium to Fe–23Cr–5Al commercial alloys has improved significantly the high-temperature oxidation resistance [15]. And enhancement on the oxidation performance of the coating $Ti_{0.7}Al_{0.3}N$ deposited on 1Cr–11Ni–2W–2Mo–V stainless steel was observed with the integration of hafnium at 800 °C in air by promoting the formation of a dense and protective alumina scale [16].

The aim of this research is to study the oxidation behavior of the alloys from Nb–Cr–Si system with 5 and 10 atomic percent of Hf in a temperature range of 700–1400 °C. This multiphase Nb-based alloy is of interest because of the formation of Laves, silicides, and Nb solid solution phases. The Nb solid solution is intended to provide tensile ductility and fracture resistance at ambient temperature. Laves and silicides are intended to provide high-temperature strength and oxidation resistance [17]. Hafnium additions are intended for improvement in both high-temperature strength and oxidation resistance, and reduce pesting susceptibility [4,5,7]. The results here have been presented for Nb–20Cr–20Si–5Hf and Nb–20Cr–20Si–10Hf alloys (compositions in atomic percent) being considered for oxidation resistance.

2. Experimental details

Two sets of Nb-based alloys were fabricated by the Ames Laboratory of Iowa State University. Alloys were prepared by arc melting technique in a high purity argon atmosphere. The ingots were re-melted several times to ensure homogeneity and were electrically discharge machined (EDM) into 5 mm × 5 mm × 5 mm samples. Before testing, all surfaces were polished to a 600 grit finish and ultrasonically cleaned in ethanol. The crucibles and caps used for the oxidation experiments were furnace dried at 300 °C for 2 h in order to remove any moisture. Then, the samples were placed in the dried crucibles with a cap on top to prevent material loss during the oxidation process.

* Corresponding author. Tel.: +1 915 747 6937; fax: +1 915 747 8036.
E-mail address: skvarma@utep.edu (S.K. Varma).

0925-8388/$ – see front matter © 2011 Elsevier B.V. All rights reserved.
doi:10.1016/j.jallcom.2011.02.174

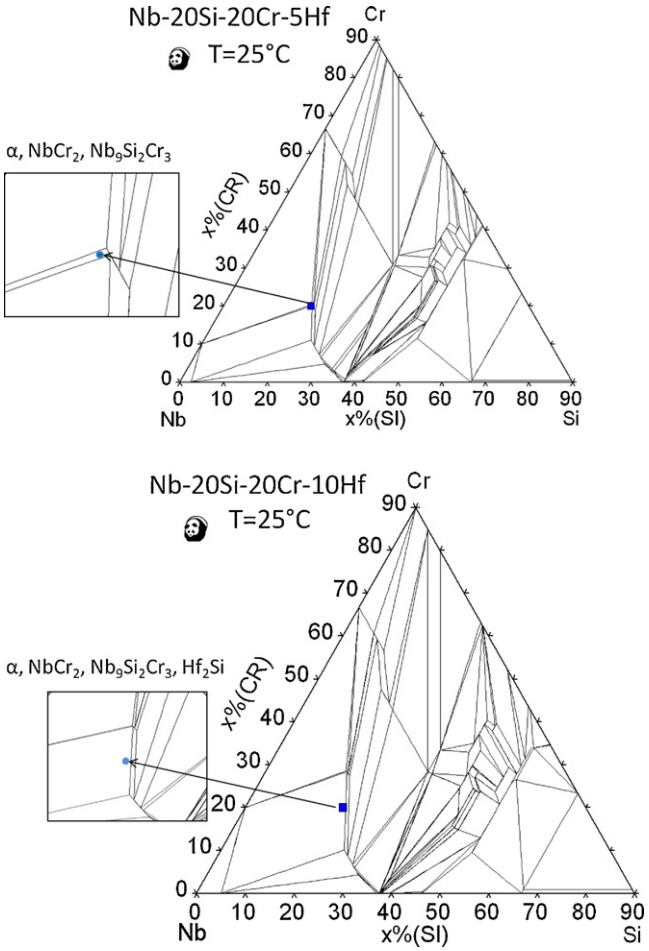

Fig. 1. Isothermal sections of the Nb–20Cr–20Si–(5,10)Hf systems calculated by PANDAT™.

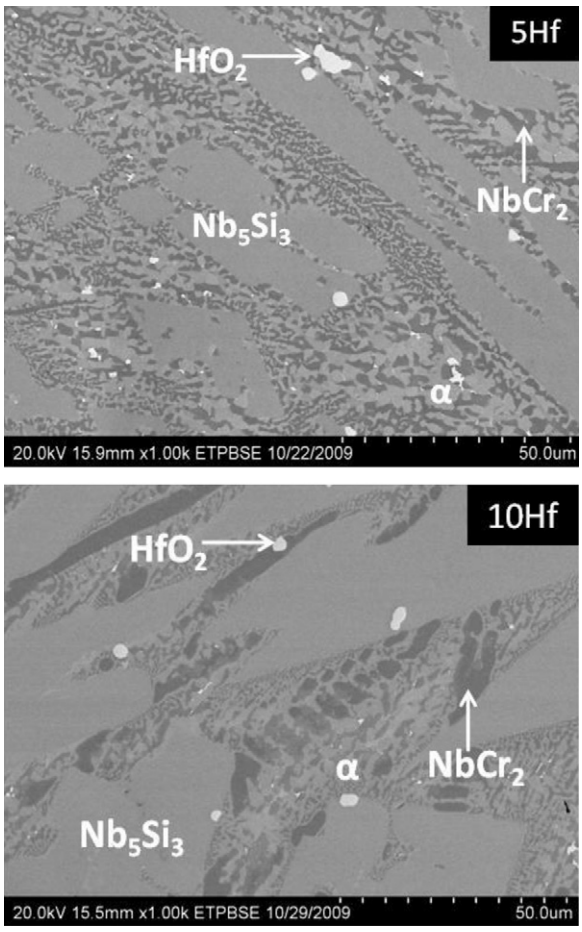

Fig. 2. As-cast microstructure of 5Hf and 10Hf alloys.

Oxidation kinetics of both alloys was studied in static air in a temperature range of 700–1400 °C using programmable furnaces. Two oxidation studies were performed: short-term oxidation (STO) and long-term oxidation (LTO). Isothermal STO consists of heating the samples for 24 h, while cyclic LTO was performed by heating for 7 cycles of 24 h each, giving a total of 168 h of air exposure. All samples were furnace cooled to room temperature from the oxidation temperatures. The weight changes were plotted as weight change per unit surface area as a function of temperature or time.

The as-cast alloys and oxidation products were characterized using scanning electron microscope (SEM) with an energy dispersive X-ray spectrometer (EDS), X-ray mapping, and X-ray diffraction (XRD). PANDAT™ 8.2 phase diagram software was used to calculate the isothermal sections of the alloys.

3. Results and discussions

3.1. As-cast characterization

Isothermal sections for the Nb–Si–Cr–Hf quaternary system were calculated based on the Nb–Si–Cr ternary system with 5 and 10 at.% fixed Hf concentrations, shown in Fig. 1. The quaternary system for Nb–20Cr–20Si–5Hf alloy indicates the presence of solid solution (α), $Nb_9Si_2Cr_3$ and Laves phase ($NbCr_2$). With the addition of 10Hf to the Nb–20Cr–20Si alloy a new silicide is added to the system corresponding to Hf_2Si composition. Fig. 2 shows the as-received microstructures for both alloys. The microstructure consists of Nb_5Si_3 (5-3 silicide, gray), $NbCr_2$ (dark gray) and HfO_2 (white). Also, there is a region that appears to be eutectic-like and consists of three phases: solid solution (α, light gray), Laves (dark gray) and 5-3 silicide (gray) phases. Also, 5-3 silicide and Laves phases rich in hafnium resulted in lighter contrast under BSE imaging conditions. Grammenos and Tsakiropoulos [3] have studied the Nb–Si–Hf–Cr systems in which the alloys presented similar microstructure as the one discuss in this paper, including Nb_{ss}, niobium-silicides, and HfO_2; Hf being a reactive element can form HfO_2 by scavenging oxygen dissolved in the alloy. The formation of $Nb_9Si_2Cr_3$ phase for 5Hf alloy and Hf_2Si phase for 10Hf were not present in the as-received microstructures for both alloys as predicted by the isothermal sections calculated by PANDAT™, this inconsistency may be attributed to the non-equilibrium processing especially during casting of the alloys.

3.2. Short-term oxidation

Fig. 3 shows the STO oxidation curves for 5Hf and 10Hf alloys obtained at temperatures ranging from 700 °C to 1400 °C. This curve represents weight gain per unit area as a function of oxidation temperature. Similar oxidation resistance has been observed for both alloys. However, the addition of 10Hf increased the weight gain at 800 °C and 1400 °C. The samples were completely oxidized at 1000 and 1100 °C for 5Hf alloy, and 900–1100 °C for 10Hf. Best oxidation resistance was observed at 700 °C for both alloys that suffered from small fine powder formation. Partial pesting behavior was observed at 800 °C with considerable amount of fine powder in the oxide product. Geng and Tsakiropoulos [2] reported pest oxidation behavior in the Nb–Ti–Si–Cr–Al–Mo system with 5Hf addition at 800 °C that was eliminated with the addition of 5Sn to the system. Suggesting that Sn in the Nb-silicide based composite played a crucial role in suppressing the pest oxidation phenomenon of the system at intermediate temperatures. Researches describe

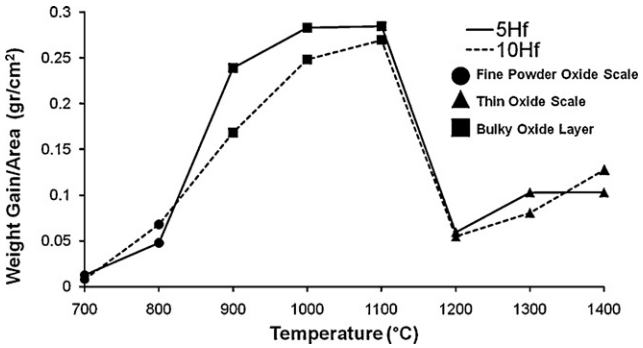

Fig. 3. Short-term oxidation (STO) curves for Nb–20Cr–20Si–5Hf and Nb–20Cr–20Si–10Hf alloys from 700 to 1400 °C.

pest oxidation as a dramatic oxidation phenomenon observed in intermetallic alloys at low temperatures (T < 850 °C) that leads to disintegration of a susceptible compound into powder [2,7]. Oxidized samples at 900–1100 °C were converted in a complete bulky oxide except for 5Hf alloy at 900 °C, which showed partial oxide/metal interface in the center surrounded by the bulky oxide. Spallation of oxide scales occurred above 1200 °C.

The microstructures of the samples exposed to isothermal conditions below 900 °C showed similar microstructure as in the as-cast conditions. However, when the samples were exposed to 1200 °C hafnia started to appear inside the α and Laves phase, and within the interface between 5-3 silicide, Laves, and α phases with different morphology from needle-like to bulky ones as shown in Fig. 4. Backscatter electron (BSE) images of microstructure formed at 1400 °C are presented in Fig. 5. Compared to the microstructure formed at 1200 °C, there was a significant increase in the volume fraction of hafnia inside the Laves at the interfaces. Also, it was observed that the Hf rich areas were not present at temperatures

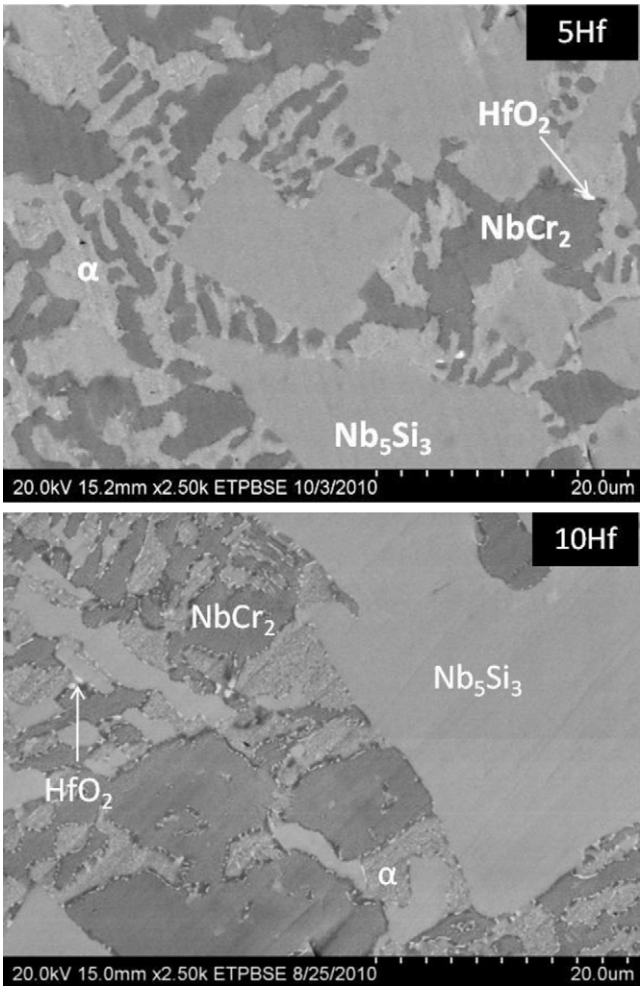

Fig. 4. The microstructure developed in 5Hf and 10Hf alloy at 1200 °C after STO.

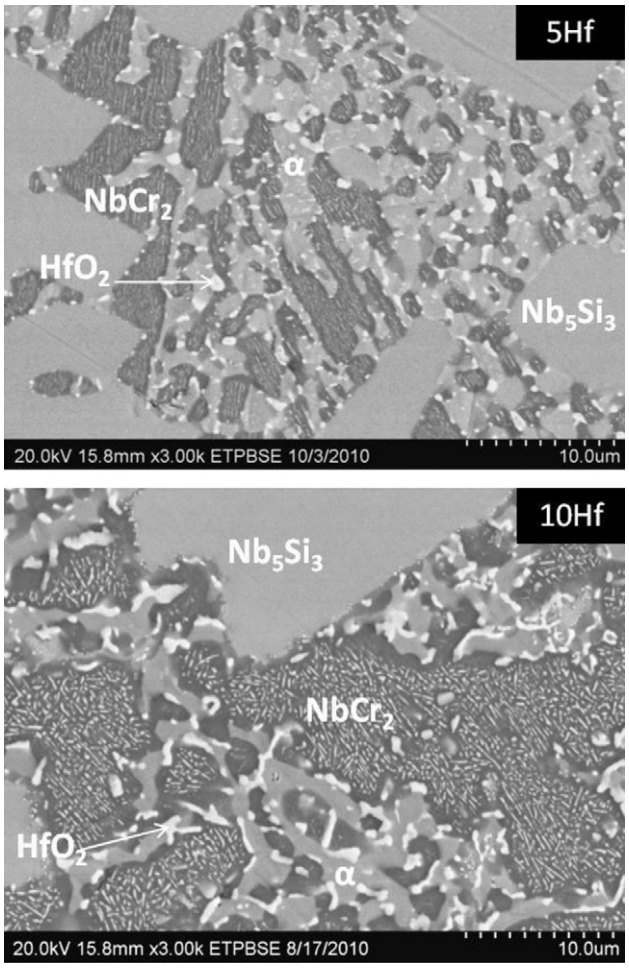

Fig. 5. The microstructure developed in 5Hf and 10Hf alloy at 1400 °C after STO.

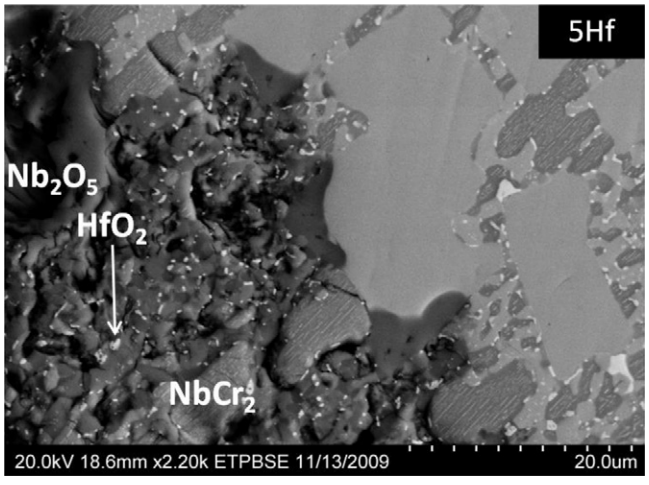

Fig. 6. Oxide metal interface in Nb–20Cr–20Si–5Hf alloy oxidized at 1400 °C for 24 h in air.

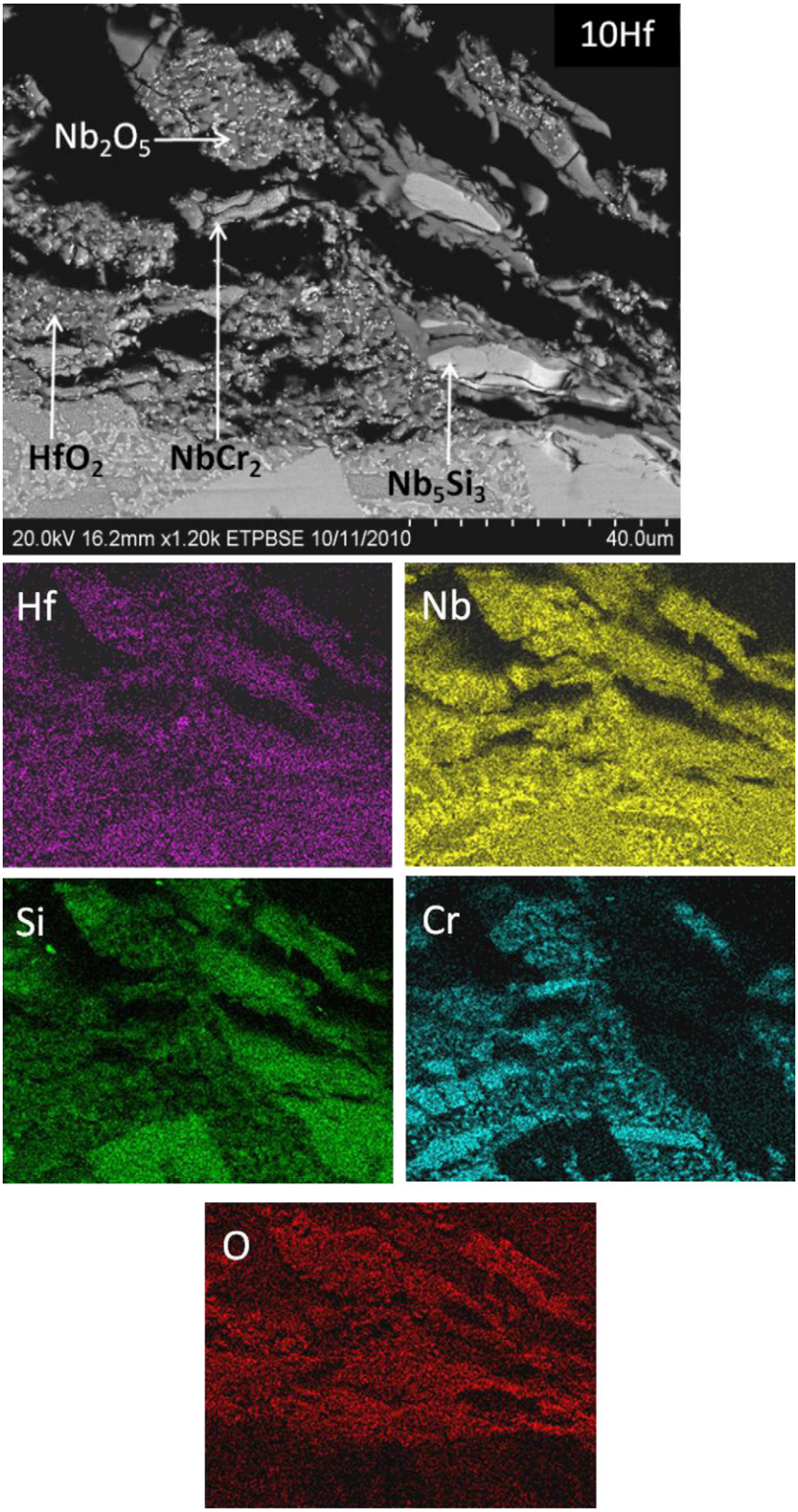

Fig. 7. Oxide metal interface in Nb–20Cr–20Si–10Hf alloy oxidized at 1400 °C for 24 h in air.

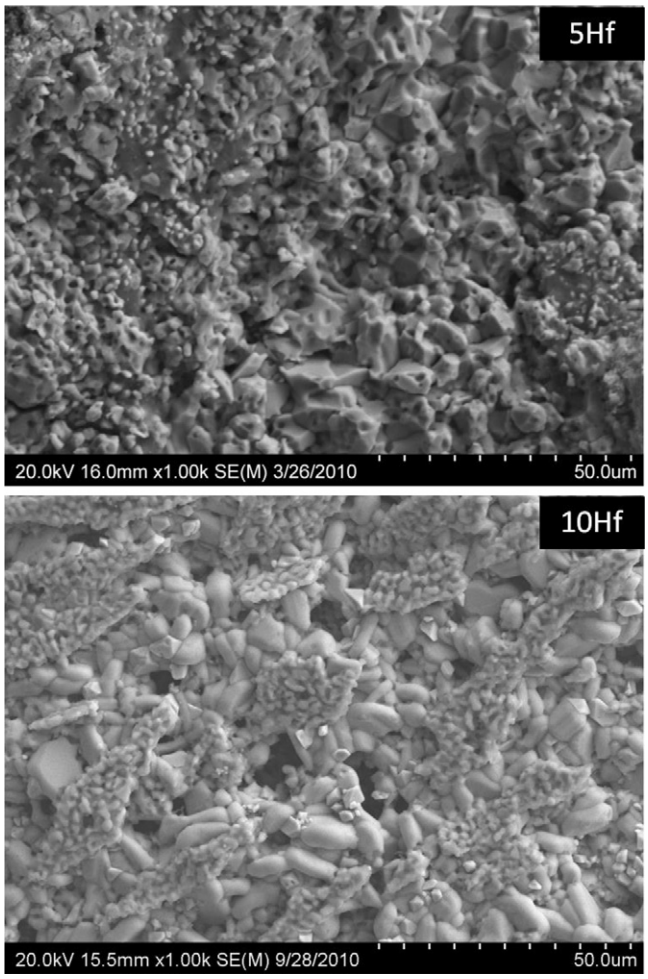

Fig. 8. SE images of the surfaces of alloys oxidized for 24 h at 1400 °C.

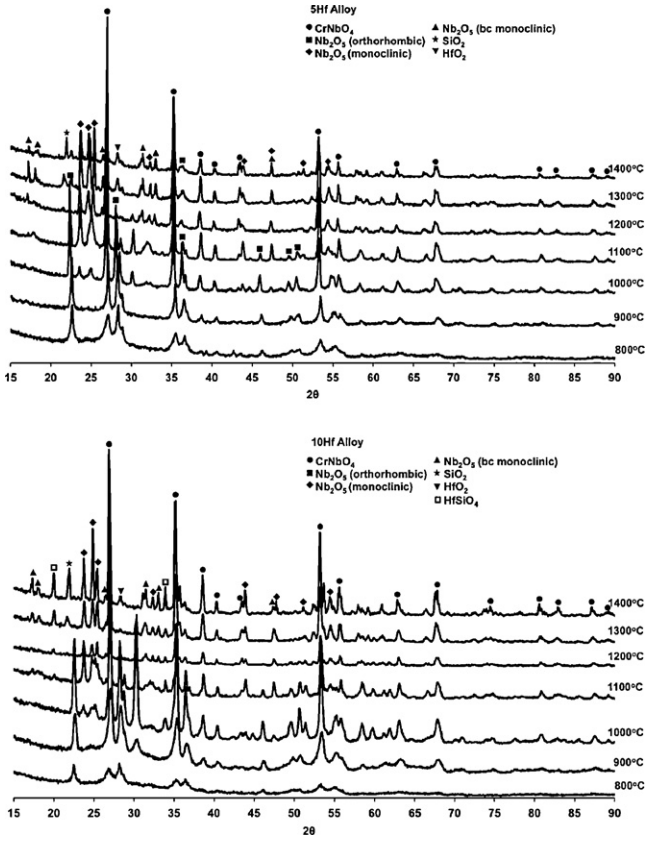

Fig. 9. XRD patterns of the oxidation products obtained from Nb–20Cr–20Si–5Hf and Nb–20Cr–20Si–10Hf alloys after 24 h of exposure.

above 1200 °C suggesting that HfO_2 formed from the Hf in solution in Nb_5Si_3 and Laves phases. This is consistent with previous studies that suggest the formation of hafnia from prior Hf rich areas of Nb_5Si_3 [2,3].

The oxide/metal interfaces developed at 1400 °C after 24 h of exposure are shown in Figs. 6 and 7 for both alloys. Porosity and cracking have been observed in the scale for both alloys that resulted in a weak adherence of the oxide scale. It appears that the main oxide is based on the stoichiometry of Nb_2O_5 as dark gray phases and portions of un-reacted intermetallic $NbCr_2$ phase. The characteristics of the oxide scale formed on the surface change with Hf content. It is important to note that un-reacted 5-3 silicide was more evident at the scale for 10Hf alloy compared to 5Hf alloy. The detail of this particular behavior has not been really understood but it indicates that the Nb solid solution phase oxidized selectively, as the Nb_5Si_3 did not oxidize. An X-ray mapping to indicate the elemental analysis in the scale is shown in Fig. 7 for 10Hf alloy. Niobium and Hafnium are almost uniformly distributed at the scale. While silicon is mostly concentrated at the un-reacted 5-3 silicide area and no homogeneous oxide layer was observed.

Fig. 8 shows the scanning electron microscope images of the morphology of the oxides formed on the metal surface at 1400 °C for 5 and 10Hf alloys. It shows that scale formed on both alloys change with hafnium content. Alloy with 5Hf addition (with better oxidation resistance at 1400 °C) have a more compact oxide scale than 10Hf alloy that exhibits a porous oxide scale with limited ability to perform as a protective barrier.

The mixture of the oxides formed has been analyzed by XRD and patterns obtained are shown in Fig. 9. The XRD technique detected Nb_2O_5, $CrNbO_4$ among other oxides. The predominant oxide formed at all temperatures was $CrNbO_4$. Three polymorphs of Nb_2O_5 were detected. Below 1000 °C orthorhombic form of Nb_2O_5 was present, while the formation of monoclinic Nb_2O_5 initiated above 1100 °C for 5Hf and 1200 °C for 10Hf alloy. Experiments indicate that the intermediate temperature range where bulky oxide formed might be associated by the formation of base-centered monoclinic Nb_2O_5 since the lattice of Nb_2O_5 expands twice when it undergoes polymorphic changes from low temperature form (α-Nb_2O_5) to β-Nb_2O_5 [18]. The SiO_2 formation has been limited to temperatures above 1300 °C.

3.3. Long-term oxidation

The samples were weighed after each cycle to construct a graph between mass gain per unit area as a function of exposure time. Fig. 10 shows oxidation curves for both alloys at 700, 800 and 1400 °C. In this study a complete oxide product was observed above 800 °C for both alloys after 168 h. Cyclic oxidation experiments revealed that both alloys exhibit a good oxidation resistance at 700 °C and 10Hf alloy shows lower weight gain per unit surface area. However, better oxidation resistance was observed for 5Hf after 168 h of exposure at 800 °C based on their weight gain per unit area, indicating the beneficial effect by the presence of hafnium at lower percentages at this temperature. The oxidation kinetics for 10Hf at 1400 °C has been observed to be comparable to 10Hf alloy at 800 °C but with an increase in the weight gain per unit surface area. On the contrary, 10Hf alloy at 1400 °C revealed a rapid oxidation rate during the first 48 h of exposure to air followed by the

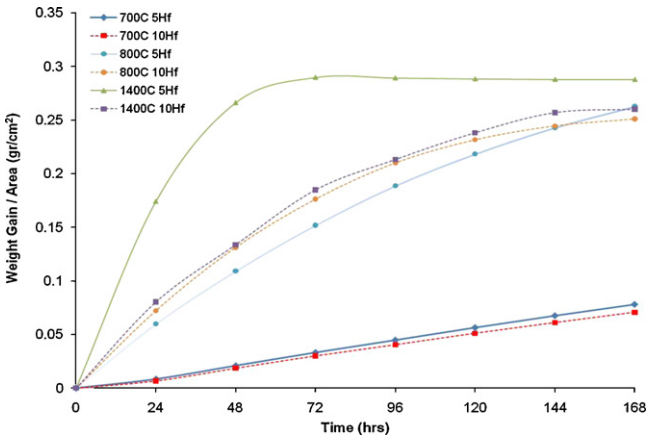

Fig. 10. Cyclic oxidation curves for 5Hf and 10Hf alloys at 700 °C, 800 °C and 1400 °C.

stabilization of the weight gain per unit area for the subsequent five cycles.

When the alloy was subjected to cyclic oxidation at 700 °C, both alloys suffered from some powder formation as well as the formation of really thin oxide scales. Fig. 11 corresponds to metal/oxide interface for 5Hf and 10Hf alloys. Cracking parallel to the substrate and porosity at the interface between the metal and the oxide scale was observed, usually caused by the stress generated by the difference in the thermal coefficients of the oxides present. The oxides formed during LTO were identified using XRD technique, EDS and BSE analysis. The oxides present at the scale were identified as Nb_2O_5 (dark gray), HfO_2 (white), and intermetallics that corresponded to un-reacted $NbCr_2$ phase. At this temperature no protective oxide layer was formed, however, the good oxidation

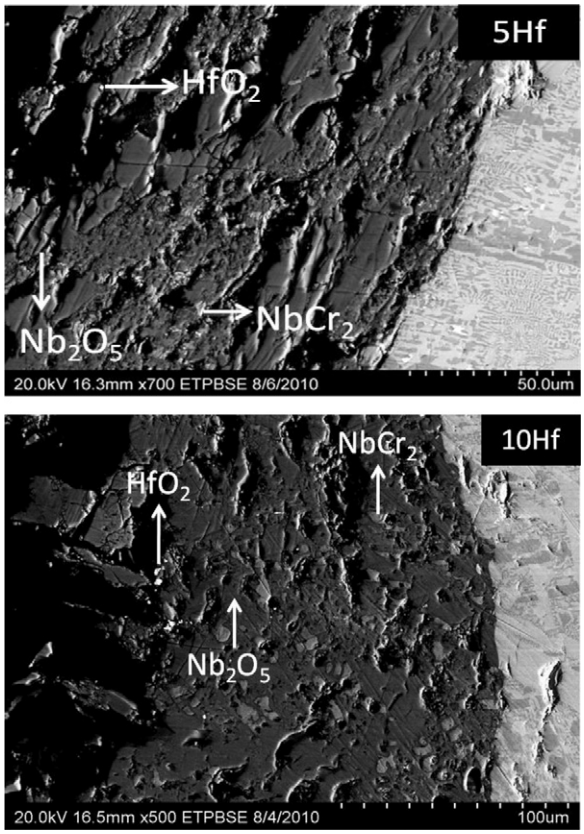

Fig. 11. Cross-section of the oxide–metal interface in Nb–20Cr–20Si–5Hf and Nb–20Cr–20Si–10Hf alloys oxidized at 700 °C after 168 h of exposure.

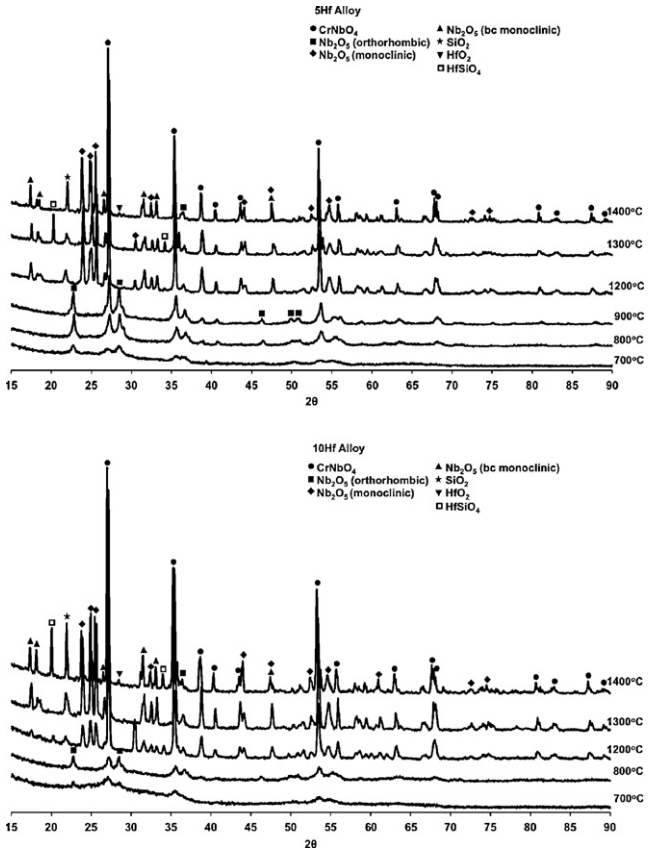

Fig. 12. XRD patterns of the oxidation products obtained from Nb–20Cr–20Si–5Hf and Nb–20Cr–20Si–10Hf alloys after168 h of exposure.

resistance is attributed to the formation of several thin scales that protected the alloy at this temperature which spall possibly as a result by the stresses created upon cooling due to the differences in the coefficients of thermal expansion between the oxides formed. Moreover, metal/oxide interfaces were observed for the samples with 10Hf addition up to 72 h while most of the Nb-based alloys with 5Hf addition oxidized complete after 68 h.

The structure of the oxides formed on the surface during cyclic oxidation was deduced from X-ray diffraction in this study; diffraction peaks from these patterns are presented in Fig. 12 in which it is observed polymorphic changes of Nb_2O_5 oxide. Below 900 °C the oxides were composed of low temperature modification of (orthorhombic) Nb_2O_5 as well as $CrNbO_4$. The products at 1200 °C are a mixture of base centered monoclinic and monoclinic modifications of Nb_2O_5 along with the formation of silicon oxide. At higher temperatures the main oxides present were the monoclinic form of Nb_2O_5 and chromium niobate. The oxidation products obtained in the Nb–Si–Cr system with Hf that included Nb_2O_5, $CrNbO_4$, and cristoballite SiO_2 are consistent with those reported by Chan [8] on different multiphase Nb-based alloys containing silicide, Laves, Nb_{ss} phases under cyclic oxidation conditions. According to Chan [8] the oxidation resistance of the Nb-based alloys was enhanced by the formation of $CrNbO_4$ instead of a combination of oxides including Nb_2O_5, $Ti_2Nb_{10}O_{29}$, and Nb_2O_5–TiO_2, and by alloys whose microstructure consisted in Nb-based silicides and Laves phase, with minimum or no Nb_{ss} phase.

4. Conclusions

1. As-cast microstructures for Nb–20Si–20Cr–(5,10)Hf alloys consist of four phases: solid solution (α), $NbCr_2$, Nb_5Si_3, and HfO_2.

The as-cast microstructure for both alloys differs from the equilibrium phases calculated by PANDAT^{TM} software.

2. Nb–20Si–20Cr–(5,10)Hf alloys exhibit good oxidation resistance at 700 °C and 800 °C and above 1200 °C when they were exposed to 24 h in static air. However, partial pesting occurred when the samples were exposed to 800 °C. However, Nb–20Cr–20Si–10Hf alloy exhibits better oxidation resistance compared to Nb–20Cr–20Si–5Hf alloy at 700 °C, 1200 °C and 1300 °C based on the weight gain per unit area.
3. Formation of base-centered monoclinic form (β-Nb_2O_5) could be responsible for the formation of bulky oxide at intermediate temperatures.
4. Alloys subjected to cyclic oxidation at 700 °C showed a good oxidation resistance with most of the sample remaining unoxidized after 168 h of exposure.

Acknowledgement

This research has been sponsored by Office of Naval Research (ONR) through the project number N00014-08-1-0506. Dr. David Shifler is the program manager.

References

[1] M.D. Morrica, S.K. Varma, Corros. Sci. 52 (2010) 2964–2972.
[2] J. Geng, P. Tsakiropoulos, Intermetallics 15 (2007) 382–395.
[3] I. Grammenos, P. Tsakiropoulos, Intermetallics 18 (2010) 242–253.
[4] P.R. Subramanian, M.G. Mendiratta, D.M. Dimiduk, JOM 48 (1) (1996) 33–38.
[5] B.P. Bewlay, M.R. Jackson, H.A. Lipsitt, Metall. Trans. A 27A (1996) 3801–3808.
[6] M.R. Jackson, B.P. Bewlay, R.G. Rowe, D.W. Skelly, H.A. Lipsitt, JOM 48 (1) (1996) 39–44.
[7] B.P. Bewlay, M.R. Jackson, J.C. Zhao, P.R. Subramanian, M.G. Mendiratta, J.J. Lewandowski, MRS Bull. (2003) 646–653.
[8] K.S. Chan, Metall. Mater. Trans. A 35A (2004) 589–597.
[9] J. Geng, P. Tsakiropoulos, G. Shao, Mater. Sci. Eng. A 441 (2006) 26–38.
[10] J. Geng, P. Tsakiropoulos, Intermetallics 15 (2007) 69–76.
[11] B.P. Bewlay, M.R. Jackson, J.C. Zhao, P.R. Subramanian, Metall. Trans. A 34A (2003) 2043–2052.
[12] B. Portillo, S.K. Varma, J. Alloys Compd. 497 (2010) 68–73.
[13] Y. Murayama, S. Hanada, STAM 3 (2002) 145–156.
[14] B.A. Pint, J. Am. Ceram. Soc. 86 (4) (2003) 686–695.
[15] T. Biegun, M. Danielewski, Z. Skrzypek, Oxid. Met. 38 (1992) 207–215.
[16] C. Feng, S. Zhu, M. Li, L. Xin, F. Wang, Oxid. Met. 71 (2009) 63–76.
[17] K.S. Chan, Oxid. Met. 61 (2004) 165–194.
[18] S.K. Varma, C. Parga, K. Amato, J. Hernandez, J. Mater. Sci. 45 (2010) 3931–3937.